Orientational Imaging of Single Molecules by Using Azimuthal and Radial Polarizations

ARTICLE *in* THE JOURNAL OF PHYSICAL CHEMISTRY B · FEBRUARY 2010

Impact Factor: 3.3 · DOI: 10.1021/jp905719b · Source: PubMed

Orientational Imaging of Single Molecules by Using Azimuthal and Radial Polarizations

Hidekazu Ishitobi,*,† Issei Nakamura,† Norihiko Hayazawa,† Zouheir Sekkat,†,‡,§,∥ and Satoshi Kawata†,‡

Nanophotonics Laboratory, RIKEN, 2-1 Hirosawa, Wako, Saitama 351-0198, Japan, Department of Applied Physics, Osaka University, 2-1 Yamadaoka, Suita, Osaka 565-0871, Japan, The Institute of Nanomaterials and Nanotechnology, iNanoTech, ENSET, Avenue de l'Armée Royale, Madinat Al Irfane, 10100 Rabat, Morocco, and Hassan II Academy of Science and Technology, Rabat, Morocco

Received: June 18, 2009; Revised Manuscript Received: January 6, 2010

Three-dimensional molecular orientations of single fluorescence molecules in polymeric thin films were measured by focused azimuthally and radially polarized light, in which we found that the fluorescence intensity was dependent on the depth position of the molecule with respect to the film surface. We found that the fluorescence intensity for a molecule which is 80 nm deep in the film excited by radial polarization is appreciably larger when compared with the fluorescence intensity for a molecule which is also excited by radial polarization but which is closer to the polymer/air interface, a feature which leads to different fluorescence intensities, under excitation by radial polarization, for molecules with the same polar orientation but with different depths inside the film. We also found that the variation of fluorescence intensity from a molecule inside an 80 nm film in radial polarization is appreciably larger compared with one in azimuthal polarization. These findings were confirmed by comparing experiments using different thickness films with theoretically calculated electric field distributions.

1. Introduction

The nanoenvironment of single fluorescence molecules affects such parameters as fluorescence lifetime, fluorescence quantum yield, triplet lifetime, and intersystem crossing yield. Measuring such parameters gives rich information on the polymer nanoenvironment at the single molecule level, such as viscosity, humidity, heterogeneity, and chemical and physical interaction between the polymer chains and the fluorescence molecule.[1−5]

It is well-known that orientations of single fluorescence molecules near an interface affect fluorescence lifetimes, fluorescence quantum yields, and fluorescence spectra.[6−8] Therefore, for investigating the nanoenvironment around single molecules, it is necessary to know their full three-dimensional (3D) molecular orientation. This is also necessary for calculating the distance between donor and acceptor molecules from measured fluorescence resonance energy transfer efficiencies because the efficiency not only depends on the distance but also relative orientations of the two molecules[9] or for investigations of orientational dynamics of single molecules for studies on biological activities.[10] In the past, different methods have been developed to determine 3D dipole orientations of single fluorescence molecules. Emission dipole orientations were determined by varying the collection angle[11] or by observing dipolar radiation patterns in defocused wide field imaging[12−21] or by a polarization analysis.[22,23] Absorption dipole orientations were determined by fluorescence rate image recorded by the raster scanning of a single molecule sample near a near-field probe[24,25] or in the focused plane of a tightly focused laser beam[26,27] where the components of the electric field distributions (E_x, E_y, and E_z) are different from each other. The 3D orientational imaging of single absorption dipoles can be also used for probing the field distribution of a tightly focused laser beam. One of the promising methods for orientational imaging of single absorption dipoles is based on annular illumination with linearly polarized light which can increase the relative weight of E_z with respect to E_x.[26] In this method, the intensity of E_z is still smaller than that of E_x ($E_z/E_x = 0.22$), a feature that disfavors the excitation of the molecules which are oriented along the Z direction, i.e., along the optical axis. Focusing radially polarized light (see Figure 1a) creates a strong E_z at the focus, and can effectively excite the molecules oriented in the Z direction.[27] However, the azimuthal angle of dipole orientation cannot be determined with high accuracy when radial polarization is used solely. More recently, both radial and azimuthal polarizations were used for studying defect luminescence of single SiO_2 nanoparticles[28] and for imaging of tautomerism in single porphyscene molecules.[29] This method was also used for scattering imaging of single Au nanorods.[30]

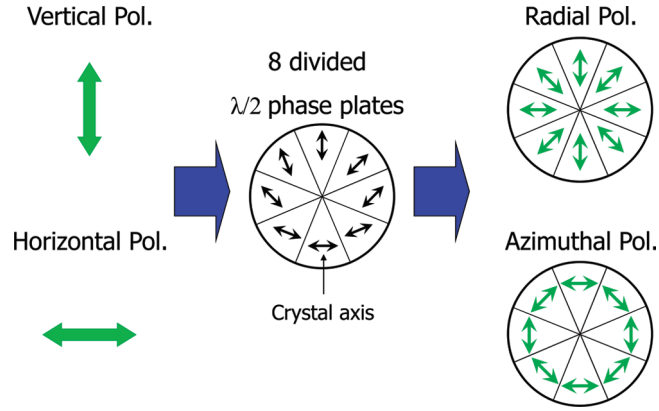

Figure 1. Divided half wave plates for generating radial and azimuthal polarizations.

* Author for correspondence. E-mail: ishitobi@riken.jp.
† RIKEN.
‡ Osaka University.
§ The Institute of Nanomaterials and Nanotechnology.
∥ Hassan II Academy of Science and Technology.

10.1021/jp905719b
Published on Web 02/10/2010

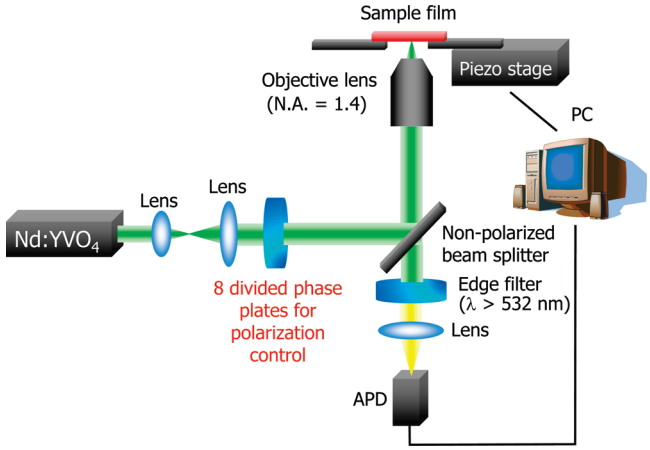

Figure 2. Optical setup for orientational imaging of single fluorescence molecules.

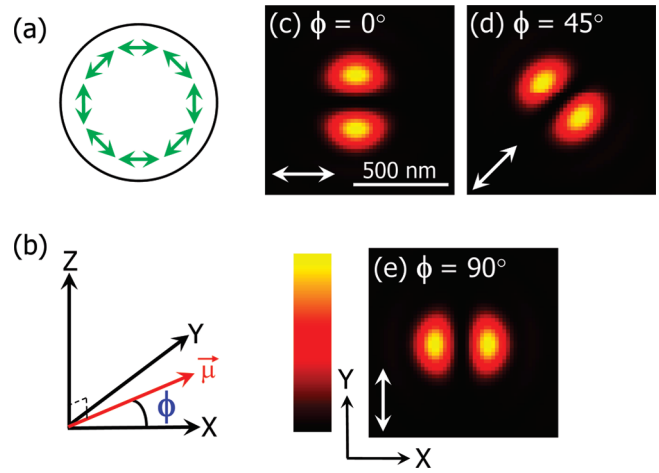

Figure 3. Calculated fluorescence intensity distribution created by a focused azimuthally polarized beam. (a) Polarization state of the azimuthal polarization in the pupil plane of an objective lens. The lines with the double arrows indicate the polarization directions. (b) Polar coordinate system. The azimuthal angle ϕ is defined by the angle between the X axis and the projection of the absorption dipole ($\vec{\mu}$) of a single molecule onto the $X-Y$ plane. (c−e) Calculated fluorescence intensity distributions in the $X-Y$ plane depending on the azimuthal angle of the single molecule.

This method has the potential to determine 3D orientations of single absorption dipoles, where the polar and azimuthal angles can be determined by radial and azimuthal polarizations, respectively. Especially this method is advantageous for measuring the polar angle of a molecule having a perpendicular orientation to the film surface with high accuracy, while it is difficult to determine such a low polar angle by the above-mentioned defocused imaging.

In this paper, we applied the method using both radial and azimuthal polarizations to 3D orientational imaging of single fluorescence molecules in polymeric films, in which we found the fluorescence intensity was dependent on the depth position of the molecule with respect to the film surface. We also found that the variation of fluorescence intensity from a molecule inside an 80 nm film in radial polarization is appreciably larger compared with one in azimuthal polarization. These findings were confirmed by comparing experiments using different thickness films with theoretically calculated electric field distributions.

2. Experiment

1,1′-Dioctadecyl-3,3,3′,3′-tetramethylindocarbocyanine perchlorate (DiI, Product No. 468495, Aldrich) was used as a fluorescence molecule because this molecule has strong photostability against photobleaching and it has been well studied.[31] Film samples were prepared by spin-coating of a ∼50 μL droplet from a chloroform solution containing the dyes with a concentration of 0.1 nM and PMMA (Product No. 200336, Aldrich, M_w = 15 000) onto a cover glass. The guest host polymer films thus prepared were heated in an oven up to 110° for 2 h to remove remnant solvents. We prepared different thickness films, i.e., 30 and 80 nm films, for confirming the dependence of the fluorescence intensity on the depth position of a molecule with respect to the film surface, which will be discussed later. The thickness was measured by an atomic force microscope.

Radial and azimuthal polarizations are created by a divided half wave plate (ZPol. Nanophoton Inc.) in which each element has different crystal axes, as shown in Figure 1. With this specially designed phase plate, vertically and horizontally polarized light can be converted to radial and azimuthal polarizations, respectively. Therefore, just by switching the input polarization state (vertical or horizontal), the output polarization state (radial or azimuthal) can be easily obtained.

A confocal fluorescence microscope was used to detect single DiI molecules (see Figure 2). The excitation laser was a frequency doubled semiconductor laser whose wavelength was 532 nm. The laser light was focused by a high N.A. objective lens (Nikon, N.A. = 1.4) onto the film surface. Fluorescence from the sample films was collected by the same objective lens and then detected by an avalanche photodiode (APD) (SPCM-AQR-14, PerkinElmer). The excitation light was cut by an edge filter (LP03-532RU-25, Semrock). This configuration can work as a confocal microscope because the detection area of the APD is small enough (200 μm × 200 μm) to realize confocality. Fluorescence images were obtained by raster scanning the sample in the $X-Y$ plane by a piezo stage (P-517, Physik Instrumente (PI)) on which the sample films were put. Incident light intensity was 150 W/cm^2, the accumulation time per one pixel was 10 ms, and the one pixel size was 30 × 30 nm.

3. Results and Discussion

For orientational imaging, prior to using radial polarization, first azimuthally polarized light was used to determine the azimuthal angle of the molecular orientation. Figure 3 shows the calculated fluorescence intensity distributions for different azimuthal orientations of a molecule excited by a focused azimuthally polarized laser beam when the absorption dipole of the single molecule is oriented at different azimuthal angles, ϕ, and a fixed polar angle of θ = 0 in the polar coordinate system (see Figures 3b and 4b) (see the Appendix for the details of the calculations). The distributions were calculated in the $X-Y$ plane, and the molecular orientation is limited in the $X-Y$ plane (θ = 0°). The focused azimuthally polarized light has only lateral components of the electric field (E_x, E_y) at the focused spot, so it is suitable for the determination of the azimuthal angle of the molecular orientation. It is found that the orientation of the fluorescence pattern is dependent on the azimuthal angle of the molecular orientation where the line between two lobes corresponds to the azimuthal angle. It is also found that the fluorescence pattern and intensity are always the same at any azimuthal angle, which allows one to determine the azimuthal angle easily. Note that the intensity of the fluorescence pattern in azimuthal polarization is also dependent on the polar angle of the molecular orientation (the fluorescence

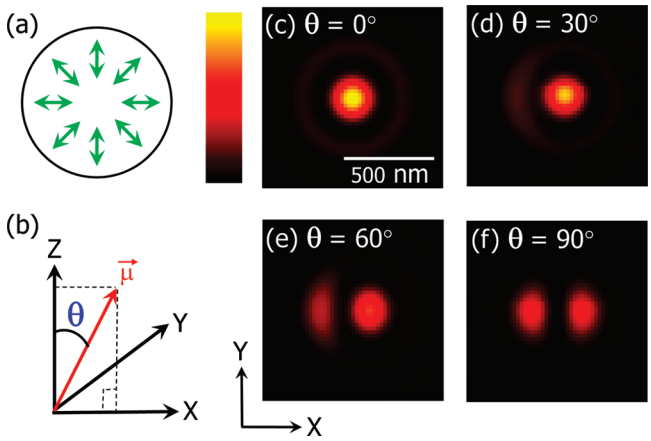

Figure 4. Calculated fluorescence intensity distribution created by a focused radially polarized beam. (a) Polarization state of the radial polarization in the pupil plane of an objective lens. The lines with the double arrows indicate the polarization directions. (b) Polar coordinate system. The polar angle θ is defined by the angle between the Z axis and the absorption dipole ($\vec{\mu}$) of a single molecule. (c−f) Calculated fluorescence intensity distributions in the $X-Y$ plane depending on the polar angle of the single molecule.

intensity is proportional to $\cos^2\theta$). After determining the azimuthal angle, radially polarized light is used to determine the polar angle. Figure 4 shows the calculated fluorescence intensity distributions for different polar orientations of a molecule excited by a focused radially polarized laser beam when the absorption dipole of the single molecule is oriented at different polar angles, θ, and a fixed azimuthal angle of $\phi = 0$ in the polar coordinate system. The distributions were calculated in the $X-Y$ plane, and the molecular orientation is limited in the $X-Z$ plane ($\phi = 0°$). It is found that the fluorescence pattern is strongly dependent on the polar angle, e.g., a single bright spot pattern corresponds to the molecule which is oriented in the Z direction (Figure 4c), and a double lobed pattern corresponds to the molecule which is oriented in the X direction (Figure 4f). It should be noted that the orientation of the fluorescence pattern is dependent on the azimuthal angle (see Figure 3 as well), which corresponds to the direction wherein the two lobes align, i.e., the line which goes through the two maximum intensity points in the two (left and right) lobes. In this case, $\phi = 0$ and the two lobes align in the same X direction. At a small polar angle such as 30° (Figure 4d), it is difficult to determine the direction wherein two lobes align, i.e., azimuthal angle, because the fluorescence pattern turns into the centrosymmetric single spot. Even at a polar angle of 60° (Figure 4e), it is not easy to define the maximum intensity point in the left lobe in the fluorescence pattern. Of course, Figures 4d and e are calculated for $\phi = 0$, but for the reasoning above, i.e., which is related to the orientation of the lobes, we assumed that these figures are for experimental observations. By making the line plot along the already determined azimuthal angle and comparing it with the theoretical calculations (see Figure 4), the polar angle can be determined. Of course, the molecule has to be locked into its nanocogent environment because the excitations with azimuthal and radial polarizations are not done simultaneously.

Figure 5 shows the orientational images of different three single DiI molecules embedded in 80 nm PMMA films obtained by azimuthal and radial polarizations, where each molecule has different molecular orientations. As predicted by the theoretical calculations shown in Figure 3, all of the fluorescence patterns obtained by azimuthal polarization (see Figure 5a−c) are similar to a pattern orientation depending on the azimuthal angle, suggesting that the imaged molecules have different azimuthal angles. Indeed, by comparing these patterns with the calculations, we found that the molecules shown in Figure 5a−c have azimuthal angles of 80, 70, and 5°, respectively. In contrast, the various fluorescence patterns which reflect different polar angles were obtained by radial polarization (see Figure 5d−f). Judging from the fluorescence pattern in Figure 5d which shows a single bright spot, it is expected that the molecule has a polar angle of $0° < \theta < 30°$. Indeed, parts c and d of Figure 4 show almost the same patterns with different intensity levels for a molecule at $0° < \theta < 30°$. It is difficult to determine such a low polar angle by using radial polarization alone. An accurate determination of the polar angle can be done by making a line plot along the already determined azimuthal angle and comparing with the theoretical calculations.

Indeed, and for the sake of illustrating the above statement, consider the following. Figure 5j shows the experimentally obtained line plot along an azimuthal angle of 80° which was already determined by the orientational image with azimuthal polarization (see Figure 5a). The line plot corresponds to the direction between the two arrows in Figure 5d. For comparison, the theoretically calculated line plot which corresponds to the direction between the two arrows in Figure 5g is also shown. The line plot was taken from the calculated fluorescence pattern when a polar angle is 20°. The intensity ratio between the left and right lobes surrounding the central peak (no central peak for larger polar angles) characterizes a polar angle (see Figure 6 which shows the calculated line plots for molecules having different polar angles). This can be better seen in Figure 5e and f, and for Figure 5d, we found that the intensity ratio of the two lobes in the experimentally obtained line plot is in good agreement with the theoretically calculated one, indicating that this molecule has a polar angle of 20°. The molecules in Figure 5b and c show the double lobed patterns with one lobe stronger than the other in radial polarization (see Figure 5e and f). By comparing the intensity ratios of the two lobes in the same manner, it is found that the molecules in Figure 5b and c have polar angles of 60 and 80°, respectively. Thus, by using both azimuthal and radial polarizations, we have succeeded in determining both azimuthal and radial angles of the molecular orientations with high accuracy.

The effect of the depth of a single fluorescence molecule on the fluorescence intensity is discussed next. Figure 7 shows the orientational images of two different individual molecules embedded in the same 80 nm PMMA film obtained by (a) azimuthal and (b) radial polarizations, respectively. The two images are shown in the same contrast. It is found from Figure 7a that the fluorescence intensities of these two molecules in azimuthal polarization are almost the same (the maximum photon counts were 300 and 350 for the left and right molecules, respectively). Theoretically, the same fluorescence intensities in azimuthal polarization indicate that these two molecules have the same polar angles, a feature which should give same fluorescence patterns with the same intensities in radial polarization. However, Figure 7b shows that the fluorescence patterns in radial polarization were the same but the fluorescence intensities were different (the maximum photon counts were 500 and 250 for the left and right molecules, respectively). We often observe this kind of intensity change in the thicker films such as 80 nm. Such an observation is due to the depth position of the fluorescence molecule inside the film. Indeed, and for analyzing such an intensity change, we calculated the field distributions of electric field components of E_x and E_z created

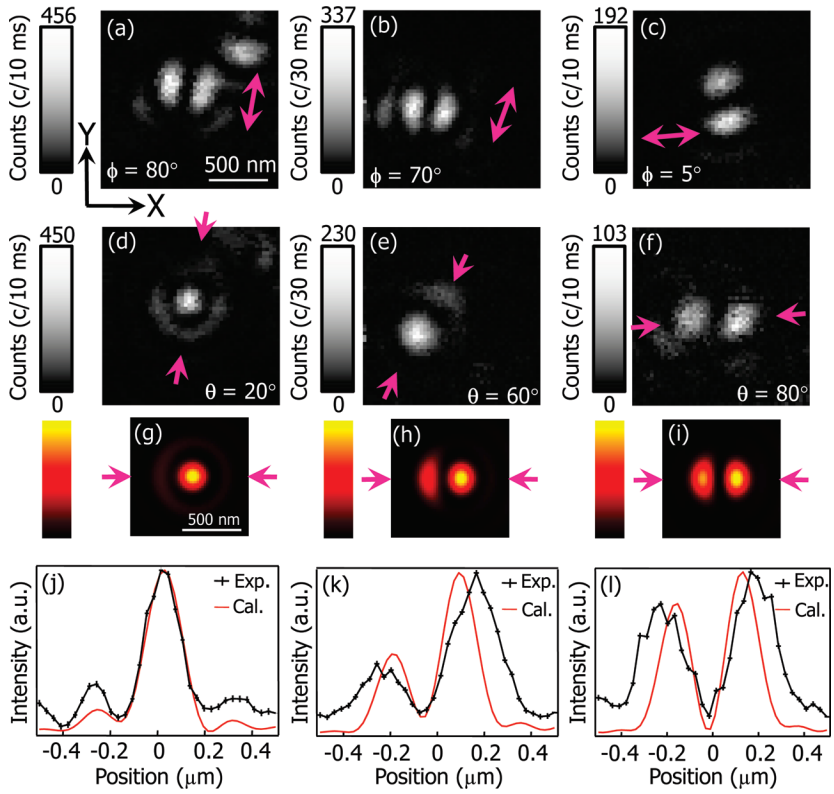

Figure 5. Orientational images of different three single DiI molecules embedded in PMMA films obtained by (a−c) azimuthal and (d−f) radial polarizations. The double arrows shown in parts a−c indicate the directions of the azimuthal angles of each molecule. (g−i) Calculated fluorescence intensity distributions in the $X-Y$ plane by radial polarization when polar angles of each single molecule are fixed at 20, 60, and 80°, respectively. (j−l) Comparisons between the experimentally obtained and theoretically calculated fluorescence intensities. The black lines with the markers (+) are the experimentally obtained line plots taken from the lines between the arrows shown in parts d−f, which lie in the directions along the azimuthal angles and go across the maximum fluorescence intensity points. The red lines are the theoretically calculated line plots taken from the lines between the arrows shown in parts g−i.

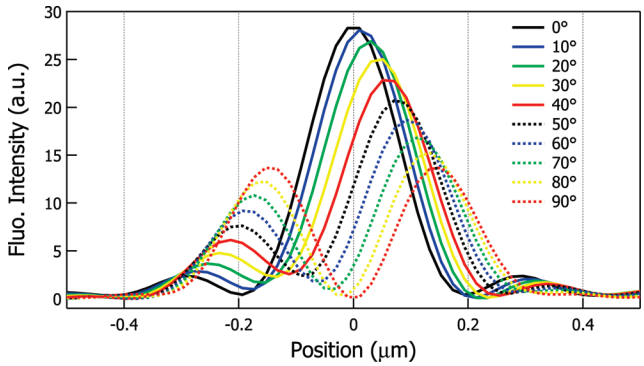

Figure 6. Calculated line plots of fluorescence intensities in radial polarization for molecules having different polar angles. The line plots are along the azimuthal angles and go across the maximum fluorescence intensity points in calculated fluorescence intensity distributions, as shown in Figure 4. The values indicate the polar angles of each molecule.

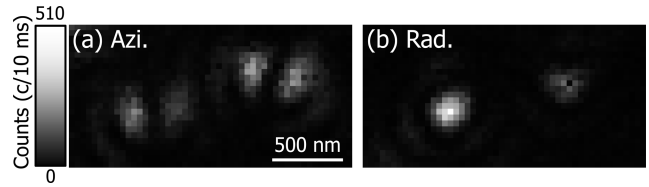

Figure 7. Orientational images of the two different individual molecules embedded in the same PMMA film obtained by (a) azimuthal and (b) radial polarizations.

by a focused radially and azimuthally polarized laser beam with an objective lens (N.A. = 1.4) in the presence of the interface between air ($n = 1.0$) and a polymer ($n = 1.5$). It is assumed that the refractive indices of the polymer and glass are the same ($n = 1.5$). Note that in the theoretical calculations discussed before (Figures 3 and 4) we assume that the single molecule is embedded in the plane 5 nm below the interface, so only the field distributions in the $X-Y$ plane 5 nm below the interface were calculated. Parts a and b of Figure 8 show the field distributions of E_x and E_z calculated in the $X-Z$ plane at $Y = 0$, respectively. The line plots of E_x and E_z which correspond to the lines at maximum intensity points ($x = 0.14$ μm for E_x and $x = 0$ μm for E_z) are also shown in Figure 8c. E_z is discontinuous at the interface between air and a polymer film due to the boundary condition. The line plots indicate the observed fluorescence intensity depends on the depth position of the target single molecule. The film thickness we used here was 80 nm, so the depth position varies from $z = 0$ to $z = -80$ nm in the coordinate. It is found from Figure 8c that E_x has the maximum value at the interface ($z = 0$) and monotonically decreases to reach the minimum value at the deepest position ($z = -80$ nm), while E_z has the minimum value at the interface and monotonically increases to reach the maximum value at the deepest position. This result suggests that the fluorescence intensity for a Z-oriented molecule which is 80 nm deep in the film excited by radial polarization is appreciably larger when compared with the fluorescence intensity for a molecule which is also excited by radial polarization but which is closer to the polymer/air interface, a feature which gives different fluorescence intensities in radial polarization for molecules with the same polar angle but with different depths in the film. Opposite behavior might be expected for X (or Y)-oriented molecules. It is also found

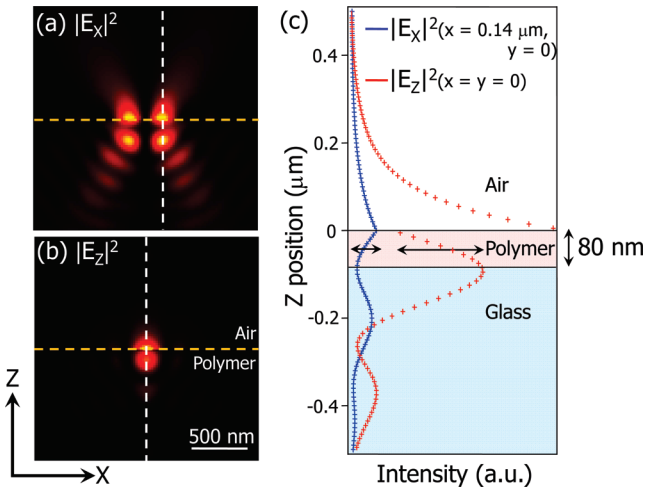

Figure 8. Calculated field distributions of electric field components of (a) E_x and (b) E_z created by a focused radially polarized laser beam with an objective lens (N.A. = 1.4), and (c) the corresponding line plots along the Z directions. The distributions are calculated in the $X-Z$ plane at $y = 0$. The yellow dashed lines indicate the interface between air ($n = 1.0$) and a polymer ($n = 1.5$). The line plots of E_x and E_z correspond to the lines which go through the maximum intensity points ($x = 0.14$ μm for E_x and $x = 0$ μm for E_z), i.e., the dashed white lines shown in parts a and b, respectively. The line plots show the dependence of the fluorescence intensities on the depth position of a single molecule. The laterally oriented lines with the double arrows shown in part c indicate the variations of the fluorescence intensities of E_x and E_z in the 80 nm film.

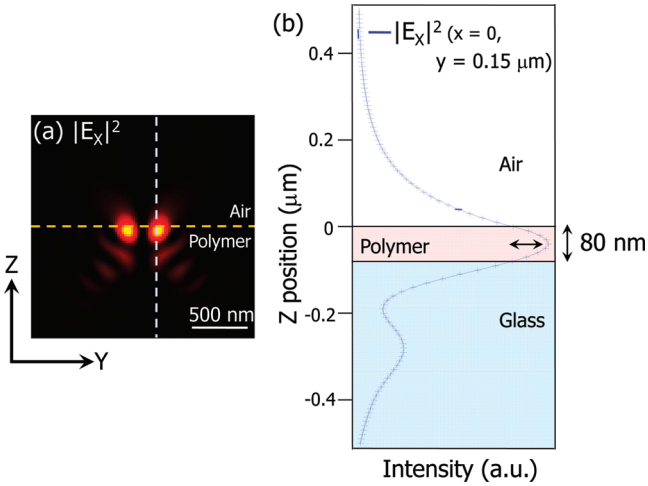

Figure 9. Calculated field distribution of an electric field component of (a) E_x created by a focused azumuthally polarized laser beam with an objective lens (N.A. = 1.4) and (b) the corresponding line plot along the Z direction. The distribution is calculated in the $Y-Z$ plane at $x = 0$. The yellow dashed line indicates the interface between air ($n = 1.0$) and a polymer ($n = 1.5$). The line plot of E_x corresponds to the line which goes through the maximum intensity point ($y = 0.15$ μm), i.e., the dashed white line shown in part a. The line plots show the dependence of the fluorescence intensity on the depth position of a single molecule. The laterally oriented line with the double arrows shown in part b indicates the variation of the fluorescence intensity of E_x in the 80 nm film.

that the variations of E_x and E_z in a range from $z = 0$ to $z = -80$ nm are ~3.9 and ~2.7, respectively (the variations are defined by $|E_{max}|^2/|E_{min}|^2$). In contrast, the variation of E_x in azimuthal polarization shown in Figure 9 is relatively small (~1.2) compared with one in radial polarization. E_x in azimuthal polarization has the maximum and minimum values at $z = -40$ nm and $z = 0$, -80 nm, respectively. These findings mean that the fluorescence intensity variation in radial polarization is large while one in azimuthal polarization is negligible. Therefore, it can be expected that the molecule shown in the left side of Figure 7 might have a deeper depth position than one in the right side.

The dependence of the fluorescence intensity on the depth position of the molecule with respect to the film surface was experimentally confirmed by using different thickness films (30 and 80 nm). Theoretically, the fluorescence intensity for a molecule excited by azimuthal polarization is dependent on the polar angle (proportional to $\cos^2\theta$), e.g., high fluorescence intensity for a molecule lying on the film surface ($\theta \sim 0°$) and low intensity for a molecule standing ($\theta \sim 90°$). In addition, as discussed above, the fluorescence intensity in azimuthal polarization for less than 80 nm film thickness is not so much dependent on the depth position of the molecule with respect to the film surface. Indeed, this trend was confirmed by the experimental observations that the fluorescence pattern in radial polarization expected from the fluorescence intensity in azimuthal polarization was in good agreement with the experimentally observed fluorescence pattern in radial polarization for both 30 and 80 nm films. Thus, if there is no dependence of the fluorescence intensity in radial polarization on the depth position of the molecule with respect to the film surface, high fluorescence intensity in azimuthal polarization should give low fluorescence intensity in radial polarization, and vice versa. In other words, the case that both fluorescence intensities in azimuthal and radial polarizations are either high or low can be attributed to differences of the position of the molecules with respect to the air−polymer interface. We picked up such a case by measuring each molecule in both radial and azimuthal polarizations. Note that the possibility that the local environment around the target molecule affects the fluorescence intensity can be ruled out by measuring many molecules for averaging. From this experiment, we found that 20 out of 55 (36%) molecules inside 80 nm films showed such a case, while 9 out of 51 (17%) molecules inside 30 nm films did. Indeed, for a 30 nm film, it is found from the calculations for radial polarization (Figure 8) that the variations of E_x and E_z in a range from $z = 0$ to $z = -30$ nm are ~1.7 and ~1.8, respectively. These variations are small compared with ones for a 80 nm film (3.9 for E_x and 2.7 for E_z), which gave the low opportunity. Note that the depth position does not affect the determination of the molecular orientation because the determination is carried out not in terms of the fluorescence intensity but in terms of the fluorescence pattern.

4. Conclusion

We measured full 3D dipole orientations of single fluorescence molecules by using both azimuthal and radial polarizations. We have succeeded in determining the 3D absorption dipole orientations of single DiI molecules embedded in PMMA films. From the theoretical calculations of the electric field distributions created by a focused radially and azimuthally polarized laser beam in the presence of the interface between air and a polymer, we found that the fluorescence intensity is strongly dependent on the depth position of the molecule and that the variation of fluorescence intensity in radial polarization is considerable compared with the one in azimuthal polarization. These findings were confirmed by comparing experimental results using different thickness films with theoretically calculated electric field distributions.

Acknowledgment. This work was supported by a Grant-in-Aid for Young Scientists (B) (No. 20760040) and a Grant-in-

Aid for Scientific Research in Priority Areas "New Frontiers in Photochromism (No. 471)" both from the Ministry of Education, Culture, Sports, Science and Technology (MEXT), Japan.

Appendix

Formulas That We Used for Calculating Fluorescence Intensity Distributions by a Radially or Azimuthally Polarized Beam Focused through a Planar Interface between Materials of Mismatched Refractive Indices. The fluorescence intensity R of a single molecule located at $\vec{r}$ is given by

$$R(\vec{r}) \propto |\vec{d}\cdot\vec{E}(\vec{r})|^2$$

where $\vec{d}$ is the unit vector along the absorption dipole moment of the molecule and $\vec{E}(\vec{r})$ is the electric field vector at the position of the molecule. When a radially polarized laser beam is incoming from material 1 to 2 and focused onto a planar interface ($X-Y$) between them by an objective lens (NA), the components of the electric field distributions created by the incident light ($\vec{E}_i$), the reflected light by the interface ($\vec{E}_r$), and the diffracted light at the interface ($\vec{E}_d$) are given by

$$\vec{E}_{i,r,d} = \left[iF_{i,r,d}(x,y,z)\frac{x}{\sqrt{x^2+y^2}}, iF_{i,r,d}(x,y,z)\frac{y}{\sqrt{x^2+y^2}}, -G_{i,r,d}(x,y,z)\right]$$

with

$$F_i(x,y,z) = \int_0^{\theta_{max}} (\cos\theta)^{3/2}\sin\theta\, J_1(k_1\sqrt{x^2+y^2}\sin\theta)\times \exp(ik_1 z\cos\theta)\,d\theta$$

$$G_i(x,y,z) = \int_0^{\theta_{max}} \sqrt{\cos\theta}(\sin\theta)^2 J_0(k_1\sqrt{x^2+y^2}\sin\theta)\times \exp(ik_1 z\cos\theta)\,d\theta$$

$$F_r(x,y,z) = \int_0^{\theta_{max}} (\cos\theta)^{3/2}\sin\theta\, r_p(\theta) J_1(k_1\sqrt{x^2+y^2}\sin\theta)\times \exp(-ik_1 z\cos\theta)\,d\theta$$

$$G_r(x,y,z) = \int_0^{\theta_{max}} \sqrt{\cos\theta}(\sin\theta)^2 r_p(\theta) J_0(k_1\sqrt{x^2+y^2}\sin\theta)\times \exp(-ik_1 z\cos\theta)\,d\theta$$

$$F_d(x,y,z) = \int_0^{\theta_{max}} \sqrt{\cos\theta}\sin\theta\sqrt{1-\left(\frac{n_1}{n_2}\sin\theta\right)^2}\times t_p(\theta) J_1(k_1\sqrt{x^2+y^2}\sin\theta)\exp\left[ik_2 z\sqrt{1-\left(\frac{n_1}{n_2}\sin\theta\right)^2}\right]d\theta$$

$$G_d(x,y,z) = \int_0^{\theta_{max}} \frac{n_1}{n_2}\sqrt{\cos\theta}(\sin\theta)^2 t_p(\theta) J_0(k_1\sqrt{x^2+y^2}\sin\theta)\times \exp\left[ik_2 z\sqrt{1-\left(\frac{n_1}{n_2}\sin\theta\right)^2}\right]d\theta$$

where θ is the incident angle of light in material 1, θ_{max} is the maximum incident angle which corresponds to ArcSin(NA/n_1), n_1 and n_2 are the refractive indices of materials 1 and 2, k_1 and k_2 are the wave numbers in materials 1 and 2, and $t_p(\theta)$ and $r_p(\theta)$ are the Fresnel coefficients for p-polarized light.[32−34] The field distributions in materials 1 and 2 are given by the interference between the incident and reflected lights ($\vec{E}_i + \vec{E}_r$) and the diffracted light ($\vec{E}_d$), respectively.

In the same matter, the components of the electric field distributions created by an azimuthally polarized beam are given by

$$\vec{E}_{i,r,d} = \left[I_{i,r,d}(x,y,z)\frac{y}{\sqrt{x^2+y^2}}, I_{i,r,d}(x,y,z)\frac{x}{\sqrt{x^2+y^2}}, 0\right]$$

with

$$I_i(x,y,z) = \int_0^{\theta_{max}} \sqrt{\cos\theta}\sin\theta\, J_1(k_1\sqrt{x^2+y^2}\sin\theta)\times \exp(ik_1 z\cos\theta)\,d\theta$$

$$I_r(x,y,z) = \int_0^{\theta_{max}} \sqrt{\cos\theta}\sin\theta\, r_s(\theta) J_1(k_1\sqrt{x^2+y^2}\sin\theta)\times \exp(-ik_1 z\cos\theta)\,d\theta$$

$$I_d(x,y,z) = \int_0^{\theta_{max}} \sqrt{\cos\theta}\sin\theta\, t_s(\theta) J_1(k_1\sqrt{x^2+y^2}\sin\theta)\times \exp\left[ik_2 z\sqrt{1-\left(\frac{n_1}{n_2}\sin\theta\right)^2}\right]d\theta$$

where $t_s(\theta)$ and $r_s(\theta)$ are the Fresnel coefficients for s-polarized light.

References and Notes

(1) Plakhotnik, T.; Donley, E. A.; Wild, U. P. Single-molecule spectroscopy. *Annu. Rev. Phys. Chem.* **1997**, *48*, 181–212.

(2) Xie, X. S.; Trautman, J. K. Optical studies of single molecules at room temperature. *Annu. Rev. Phys. Chem.* **1998**, *49*, 441–480.

(3) Moerner, W. E. A Dozen Years of Single-Molecule Specroscopy in Physics, Chemistry, and Biophysics. *J. Phys. Chem. B* **2002**, *106*, 910–927.

(4) Moerner, W. E.; Fromm, D. P. Methods of single-molecule fluorescence spectroscopy and microscopy. *Rev. Sci. Instrum.* **2003**, *74*, 3597–3619.

(5) Kulzer, F.; Orrit, M. Single-Molecule Optics. *Annu. Rev. Phys. Chem.* **2004**, *55*, 585–611.

(6) Macklin, J. J.; Trautman, J. K.; Harris, T. D.; Brus, L. E. Imaging and Time-Resolved Spectroscopy of Single Molecules at an interface. *Science* **1996**, *272*, 255–258.

(7) Vallée, R.; Tomczak, N.; Gersen, H.; van Dijk, E. M. H. P.; García-Parajó, M. F.; Vancso, G. J.; van Hulst, N. F. On the role of electromagnetic boundary conditions in single molecule fluorescence lifetime studies of dyes embedded in thin films. *Chem. Phys. Lett.* **348**, 161–167.

(8) Kreiter, M.; Prummer, M.; Hecht, B.; Wild, U. P. Orientation dependence of fluorescence lifetimes near an interface. *J. Chem. Phys.* **2002**, *117*, 9430–9433.

(9) Ha, T.; Enderle, T.; Ogletree, D. F.; Chemla, D. S.; Selvin, P. R.; Weiss, S. Probing the interaction between two single molecules: Fluorescence resonance energy transfer between a single donor and a single acceptor. *Proc. Natl. Acad. Sci. U.S.A.* **1996**, *93*, 6264–6268.

(10) Forkey, J. N.; Quinlan, M. E.; Shaw, M. A.; Corrie, J. E. T.; Goldman, Y. E. Three-dimensional structural dynamics of myosin V by single-molecule fluorescence polarization. *Nature* **2003**, *442*, 399–404.

(11) Plakhotnik, T.; Moerner, W. E.; Palm, V.; Wild, U. P. Single Molecule Spectroscopy: maximum emission rate and saturation intensity. *Chem. Phys. Lett.* **1995**, *114*, 83–88.

(12) Jansny, J.; Sepio, J. Single molecules observed by immersion mirror objective. A novel method of finding the orientation of a radiating dipole. *Chem. Phys. Lett.* **1997**, *273*, 439–443.

(13) Sepio, J.; Jansny, J.; Keller, J.; Wild, U. P. Single molecules observed by immersion mirror objective. The orientation of terrylene molecules via the direction of its transition dipole moment. *Chem. Phys. Lett.* **1997**, *273*, 444–448.

(14) Dickson, R. M.; Norris, D. J.; Moerner, W. E. Simultaneous Imaging of Individual Molecules Aligned Both Parallel and Perpendicular to the Optic Axis. *Phys. Rev. Lett.* **1998**, *81*, 5322–5325.

(15) Bartko, A. P.; Dickson, R. M. Three-Dimensional Orientations of Polymer-Bound Single Molecules. *J. Phys. Chem. B* **1999**, *103*, 3053−3056.

(16) Bartko, A. P.; Dickson, R. M. Imaging Three-Dimensional Single Molecule Orientations. *J. Phys. Chem. B* **1999**, *103*, 11237–11241.

(17) Böhmer, M.; Enderlein, J. Orientational imaging of single molecules by wide-field epifluorescence microscopy. *J. Opt. Soc. Am. B* **2003**, *20*, 554–559.

(18) Lieb, M. A.; Zavislan, J. M.; Novotny, L. Single-molecule orientations determined by direct emission pattern imaging. *J. Opt. Soc. Am. B* **2004**, *21*, 1210–1215.

(19) Patra, D.; Gregor, I.; Enderlein, J. Image Analysis of Defocused Single-Molecule Images for Three-Dimensional Molecules Orientation studies. *J. Phys. Chem. A* **2004**, *108*, 6836–6841.

(20) Uji-i, H.; Melnikov, S. M.; Deres, A.; Bergamini, G.; Schryver, F. D.; Herrmann, A.; Müllen, K.; Enderlein, J.; Hofkens, J. Visualizing spatial and temporal heterogeneity of single molecule rotational diffusion in a glassy polymer by defocused wide-field imaging. *Polymer* **2006**, *47*, 2511–2518.

(21) Dedecker, P.; Muls, B.; Deres, A.; Uji-i, H.; Hotta, J.-i.; Sliwa, M.; Soumillion, J.-P.; Müllen, K.; Enderlein, J.; Hofkens, J. Defocused Wide-field Imaging Unravels Structural and Temporal Heterogeneity in Complex Systems. *Adv. Mater. A* **2009**, *21*, 1079–1090.

(22) Fourkas, J. T. Rapid determination of the three-dimensional orientation of single molecules. *Opt. Lett.* **2001**, *26*, 211–213.

(23) Hohlbein, J.; Hübner, C. G. Simple scheme for rapid three-dimensional orientation determination of the emission dipole of single molecules. *Appl. Phys. Lett.* **2005**, *86*, 121104.

(24) Betzig, E.; Chichester, R. J. Single Molecules observed by Near-Field Scanning Optical Microscopy. *Science* **1993**, *262*, 1422−1425.

(25) Frey, H. G.; Witt, S.; Felderer, K.; Guckenberger, R. High-Resolution Imaging of Single Fluorescent Molecules with the Optical Near-Field of a metal tip. *Phys. Rev. Lett.* **2004**, *93*, 200801.

(26) Sick, B.; Hecht, B.; Novotny, L. Orientational Imaging of Single Molecules by Annular Illumination. *Phys. Rev. Lett.* **2000**, *85*, 4482–4485.

(27) Novotny, L.; Beversluis, M. R.; Youngworth, K. S.; Brown, T. G. Longitudinal Field Modes Probed by Single Molecules. *Phys. Rev. Lett.* **2001**, *86*, 5251–5254.

(28) Chizhik, A. M.; Chizhik, A. I.; Gutbrod, R.; Meixner, A. J.; Schmidt, T.; Sommerfeld, J.; Huisken, F. Imaging and Spectroscopy of Defect Liminescence and Electron-Phonon Coupling in Single SiO_2 Nanoparticles. *Nano. Lett.* **2009**, *9*, 3239–3244.

(29) Piwo, H.; Hartschuh, A.; Urba, N.; Pietraszkiewicz, M.; Sepio, J.; Meixner, A. J.; Waluk, J. Polarized Spectroscopy Studies of Single Molecules of Porphycenes: Tautomerism and Orientation. *J. Phys. Chem. C* **2009**, *113*, 11514–11519.

(30) Failla, A. V.; Qian, H.; Qian, H.; Hartschuh, A.; Meixner, A. J. Orientational Imaging of Subwavelength Au Particles with High Order Laser Modes. *Nano Lett.* **2006**, *6*, 1374–1378.

(31) Renn, A.; Seelig, J.; Sandoghdar, V. Oxygen-dependent photochemistry of fluorescent dyes studied at the single molecule level. *Mol. Phys.* **2006**, *104*, 409–414.

(32) Biss, D. B.; Brown, T. G. Cylindrical vector beam focusing through a dielectric interface. *Opt. Express* **2001**, *9*, 490–497.

(33) Helseth, L. E. Roles of polarization, phase and amplitude in solid immersion lens systems. *Opt. Commun.* **2001**, *191*, 161–172.

(34) Török, P.; Varga, P.; Laczik, Z.; Booker, G. R. Electromagnetic diffraction of light focused through a planar interaface between materials of mismatched refractive indices: an integral representation. *J. Opt. Soc. Am. A* **1995**, *12*, 325–332.

JP905719B